8-12-2013

Electromagnetic Stimulation of Transport in Water for Geoenvironmental Applications

A. Farid
Boise State University

M. Azad
Boise State University

J. Browning
Boise State University

Elisa H. Barney Smith
Boise State University

Electromagnetic Stimulation of Transport in Water for Geoenvironmental Applications

A. Farid, M. Azad, J. Browning, and E. Barney-Smith
Boise State University, USA

Abstract— Air sparging is a popular soil remediation technique that enables the removal of contaminants by diffusing air into saturated zones of soil. The removal process is, however, slow. The goal of this work is to study the effect of electromagnetic (EM) waves — with minimal heat generation — on transport mechanisms such as diffusion, in order to improve airflow or contaminant transport and expedite the cleanup process using air sparging or similar technologies. This effect is studied through an experimental setup that examines the diffusion of a nonreactive dye in water under EM waves at a range of frequencies between 50 and 200 MHz. The electric field was simulated using COMSOL Multiphysics for better 3D visualization and analysis and then validated using experimental measurements. A dielectrophoretic study was performed using the simulated electric field. Various dye flow under EM stimulation at different frequencies were compared. At 65 MHz and 76 MHz, the dye flow was in the direction of the dielectrophoretic forces, which is believed to be the governing mechanism for dye transport.

1. INTRODUCTION

Remediation of contaminated soil/groundwater has become an area of interest in recent decades. Several remediation techniques have been used for removal of the contaminants, among which air sparging [1] is very popular. In-situ air sparging (AS) is a technique in which air or oxygen is injected into water-saturated zones in order to remove organic contaminants by a combination of volatilization and aerobic biodegradation processes. The contaminant-free air injected into the saturated zones of the subsurface enables the phase transfer of organic contaminants from a dissolved or adsorbed state to a vapor phase. Despite the impressive results, the effectiveness of air sparging is limited because of its semi-random remediation process [2]. Air can flow more easily in partially saturated media compared to water-saturated ones, resulting in airflow limited to initial randomlyformed air channels. An advantage of EM over other enhancement methods, such as the use of direct or alternating current (DC or AC), is that EM waves can be applied at proper frequencies (lower MHz) and lower EM power and, therefore, would dissipate a small amount of energy in the medium and would not alter the pH of the environment. The transport of a nonreactive inert dye in water is studied as a visible analogy to the air or contaminant flow in saturated media. The goal of this work is to study the effect of electromagnetic waves on transport mechanisms in saturated media at frequencies where heat generation is minimal. The main objective of this work is to find the governing phenomenon that directs the flow of the dye when EM stimulation is applied. Dielectrophoresis [3] is specifically investigated as a potential governing mechanism behind this effect. Studying the relationship between the magnitude of the EM power and the transport rate, as a representative of the transport rate, is another objective of this work.

2. METHODOLOGY, EXPERIMENTATION, AND SIMULATION

The experimental setup consists of a 40-cm × 40-cm × 40-cm acrylic box (Figure 1) and a 38-cm × 38-cm × 38-cm RF (radio-frequency) resonant cavity, filled with water. The cavity structure is built using copper mesh screens instead of solid copper plates to enable imaging and visualization. The opening diameter of the copper mesh is ~ 3 mm (1/8 inch), which is much smaller than the wavelength of the applied 50–200 MHz frequency waves in water (≈ 160 mm–660 mm). A coaxial loop antenna coupled to the resonant cavity and connected to the EM source launches EM waves into the medium. The antenna is made of an RG8 coaxial cable. The outer conductor of the cable is electrically grounded at both ends of the cable, sharing the same electric ground as the cavity. The inner conductor passes through a brass piece soldered to the top copper boundary, hence, sharing the same electric ground as the outer conductor, to provide electrical continuity to the resonant cavity. A continuous wave (CW) radio-frequency signal was generated using an HP E4400B signal generator and amplified using a Model 100 LMB amplifier, manufactured by Amplifier Research. To maximize the amplifier output forward power to be input into the testing medium, a matching network was used (See [4] for more information).

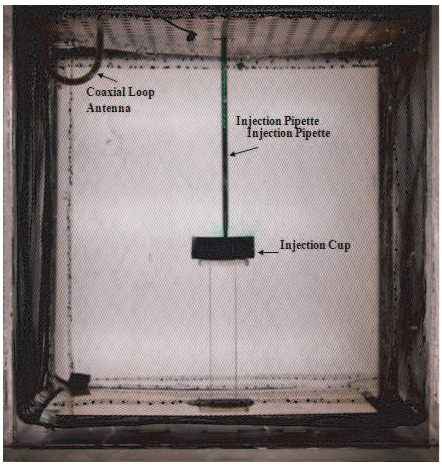

Figure 1: Medium under test for the modified setup showing the acrylic box, resonant cavity filled with water, injection cup, injection pipette, and loop antenna.

An inert, nonreactive, water-based dye (a green McCormick food-coloring dye) was used as the diffusing matter to allow the visualization of the transport inside the medium. A clear acrylic table was built to allow the introduction of the dye close to the center of the medium (far from the cavity boundaries). A circular plastic cup with a radius of 30 mm was glued to the top plate of the injection table. The cup is used to hold the dye during the initial injection and prevent the dye from descending off the injection table down to the bottom of the box. Digital imaging was used to analyze the transport of the dye to determine the EM-stimulation effect. Images were taken using a Cannon Rebel T2i 18-MegaPixel digital camera. Images were taken at 30-second intervals for this experiment. The pixel values of the two-dimensional (2D) digital images correlate to the dye concentration integrated along corresponding lines of sight.

The electric field is mapped in the region under test using a 50-Ω, RG-402, coaxial probe controlled by a three-dimensional (3D) translation table. The probe is connected to a spectrum analyzer and is moved to the nodes of a desired 3D grid. The monopole probe is vertically polarized. However, a full 3D vector electric field is necessary to understand the correlation between the

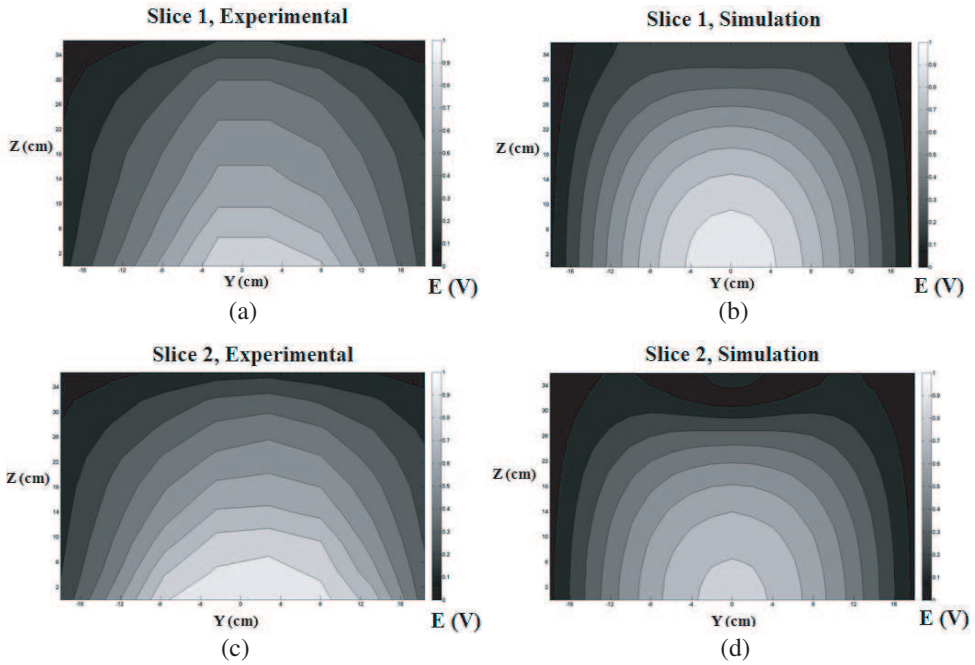

Figure 2: Normalized electric field map: (a) Slice 1, experimentally measured; (b) Slice 1, simulated; (c) Slice 2, experimentally measured; and (d) Slice 2, simulated.

RF radiation pattern and the dye transport. Therefore, the electric field pattern is simulated at various frequencies using the COMSOL software, and its Z component is validated against the experimentally mapped electric field. Figure 2 shows the measured and simulated contour maps on two depth slices at 65 MHz. In order to investigate the effect of temperature on the dye flow, the temperature of the water close to the antenna body was recorded at different EM-stimulation frequencies.

3. RESULTS AND DISCUSSION

3.1. Unstimulated Tests

After complete injection of the dye, small portions of the dye rose from the cup and then descended downward because the dye density was slightly larger than that of water ($1\,\mathrm{g/cm^3}$). There was a relatively random time interval (5 to 12 minutes) at which the dye rose out of the cup. However, approximately 1 hour past the beginning of the experiment, this time interval decreased, and more continuous risings were observed. Figure 3(a) shows an example of the dye transport in an unstimulated test.

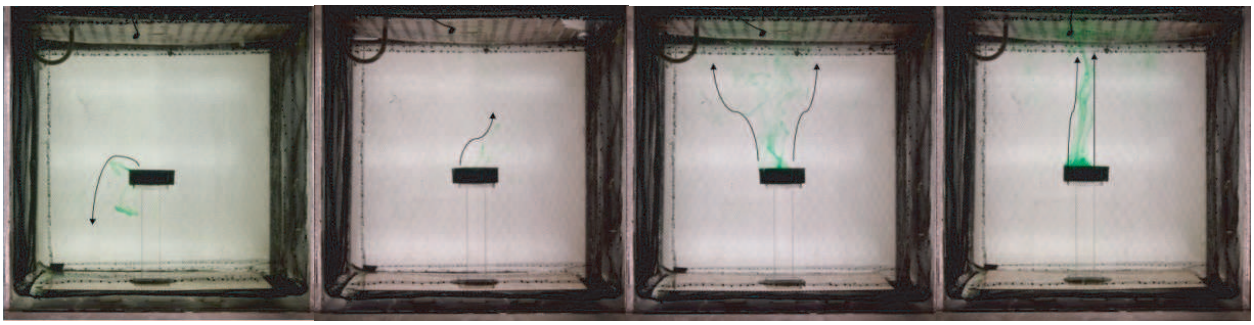

(a) (b) (c) (d)

Figure 3: (a) Dye transport during: (a) an unstimulated test; dye randomly rises out of injection cup and descends; and dye flow in an EM-stimulated experiment at 65 MHz frequency after 20 minutes of stimulation and at the power level of: (b) 10 W, (c) 20 W, and (d) 30 W. Dye rises out of injection cup toward top boundary.

3.2. Stimulated Tests

When the medium was stimulated at the frequency of 65 MHz, there was an upward flow of the dye. Portions of the dye rose out of the cup and moved upward toward the top boundary of the resonant cavity. After reaching the top boundary, the dye spread horizontally in random directions. The stimulated experiment was performed at 10, 20, and 30 W to investigate the effect of the power level. Increasing the EM power increased the upward dye flow. Figures 3(b), 3(c), and 3(d) illustrate the flow of the dye 20 minutes after the dye injection at power magnitudes of 10, 20, and 30 W, respectively. The threshold of power needed to electromagnetically induce the upward dye transport is $P = 10\,\mathrm{W}$ at the frequency of $f = 65\,\mathrm{MHz}$.

3.3. Frequency Effect

Although only the 65 MHz simulation was successfully validated experimentally, the experiment was repeated for other frequencies as well. The choice of the frequency was based on the quality of the impedance-matching achieved that was monitored by the spectrum analyzer. As a result, several tests were performed at 60, 69, 75, and 77 MHz at an RF power of 30 W. Unlike the tests performed at 65 MHz, during the stimulation at these other frequencies — except for 75 MHz — the flow of the dye was observed to be similar to the unstimulated tests. In other words, the stimulation had no apparent effect on the flow of the dye. At 75 MHz, the dye remained inside the cup for as long as the medium was stimulated and the power was above 3 W. The simulated electric-field pattern seems to support this phenomenon according to a potential dielectrophoretic nature. However, the experimental electric-field measurements showed no consistency with the simulation.

3.4. Temperature Effect

The change of temperature over time was monitored at various frequencies at a point 1 cm from the center of the loop antenna, where the strongest temperature rise was expected due to resistive heat

generation at the proximity to the heat source (i.e., loop antenna). As expected, the temperature slightly increased for all the frequencies over time. The maximum change in temperature within the period of stimulation was less than 1°C for all frequencies. The observed pattern of rise in the temperature was the same for all frequencies, while the electric-field radiation pattern and dye flow were different for 65 MHz, 75 MHz, and other frequencies. This suggests that the flow of the dye is not dominated by a convective flow (due to thermal effects) and is due to the electromagnetic field.

3.5. Electric-field Pattern Effect and Governing Mechanism

The validated simulated electric field, containing the X, Y, and Z components of the electric field at nodes spaced on a 2-cm grid within the cavity, was exported into MATLAB. A script (*m.file*) was developed in MATLAB using a forward finite difference method to calculate the dielectrophoretic force based on Equation (1).

$$\begin{aligned}\vec{F}_{DEF} &= 2\pi r^3 \varepsilon_m^* \mathrm{Re}\left\{\frac{\varepsilon_p^* - \varepsilon_m^*}{\varepsilon_m^*}\right\} \vec{\nabla} |E|^2_{(i,j,k)} \\ &= 2\pi r^3 \varepsilon_m^* \mathrm{Re}\left\{\frac{\varepsilon_p^* - \varepsilon_m^*}{\varepsilon_m^*}\right\} \left(\frac{|E|^2_{i,j+1,k} - |E|^2_{i,j-1,k}}{2dx} + \frac{|E|^2_{i+1,j,k} - |E|^2_{i-1,j,k}}{2dy} + \frac{|E|^2_{i,j,k+1} - |E|^2_{i,j,k-1}}{2dz} \right) \quad (1)\end{aligned}$$

Three matrices of the three components of the gradient of the squared electric field ($\nabla|E|^2$) were computed. However, the dye concentration at each node within images represents the concentration integrated over the line of sight (in the Y direction, i.e., perpendicular to the image). Hence, the X and Z components of the gradient of the squared electric field were integrated over the Y-axis. Figures 4(a) and 4(b) represent the contour map of the Z and X components of the $\nabla|E|^2$ vector, respectively.

According to Figure 4(a), the Z-component of $\nabla|E|^2$ is negative with an increasing magnitude toward the top. As a result, because of the smaller dielectric constant of dye compared to that of water, the direction of the dielectrophoretic forces are in the positive Z direction (i.e., upward) at 65 MHz. This result is in agreement with the results from the experimental field investigation as well.

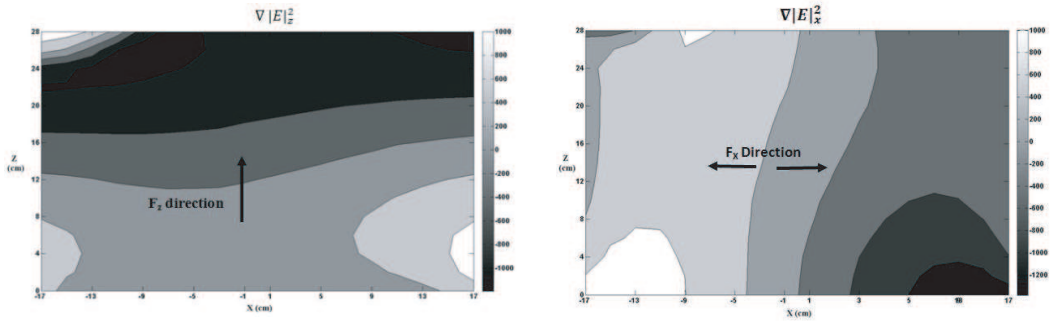

(a) (b)

Figure 4: Contour map of the simulated $\nabla|E|^2$ ($\mathrm{V^2/m^3}$) according to COMSOL Multiphysics results at 65 MHz: (a) Z component and (b) X component.

On the other hand, the X-component of the $\nabla|E|^2$ vector creates a force dragging the dye toward the side walls of the cavity. However, the magnitude of the forces in the X direction is almost 1/2 of the magnitude of the vertical forces. As a result, the upward flow of the dye dominates the horizontal flow except near the top boundary, where the upward flow has slowed or stopped. Since the dye has a flow moving both right and left after it reaches the top boundary, the observed flow near the top boundary can be interpreted as a mix of dielectrophoresis and diffusion.

3.6. Digital Analysis and Evaluation

Digital-image analysis was performed to extract quantifiable information from images of dye transport in RAW format. RAW-format images were then converted into the TIFF format and imported into MATLAB in matrix format. The averaged, background image (containing everything but the dye) was subtracted from every other image, leaving only the transporting dye. The elements of the resulting matrices represent the intensity of pixels at different locations in the box as a representative of dye concentration. Following analyses were then performed.

3.6.1. Pixel Intensity Summation

A zone shown in Figure 5(a) was selected to measure the amount of dye that had left the injection cup or the main finger formed in each test. The summation was performed on the set of the experiments performed at 65 MHz (10 W, 20 W, and 30 W) as well as for the test performed at 75 MHz (30 W) and the unstimulated test. Figure 6 shows the plot of the summation of pixel intensities over time for these tests. Because no dye transport was observed for the tests performed at 75 MHz, it was, hence, expected that the summation of pixel values for this test be constant over time. However, the plot shows some variation over time attributed to the errors associated with the background noise. In general, the average value did not increase or decrease. The similar range of concentration data associated with the unstimulated test and the stimulated test at 10 W proves that the amount of the dye entering this zone was not large enough to overcome the noise. In summary, the change of the sum of pixel intensities over time for the unstimulated test, stimulated test at 75 MHz (even at 30 W of power), and 65 MHz (with a power less than 10 W) followed the same pattern with the average unchanged. The plot of pixel values over time for the stimulated tests of 65 MHz at 20 W and 30 W, on the other hand, shows different results. The sum of adjusted pixel intensities increased over time for these two tests, meaning pixels became darker. This refers to the presence of more dye in the upper region. In order to quantify the variations in the sum of pixel values over time for each test, the relative change (%) of the summation was also calculated. Therefore, the last three datasets (at $t = 105$ min., 106.5 min., and 108 min. after the beginning of the stimulation) were averaged and subtracted from the initial dataset ($t = 0$ min.) of the curves of Figure 6(a). The relative change (%) was calculated and plotted versus power (Figure 6(b)).

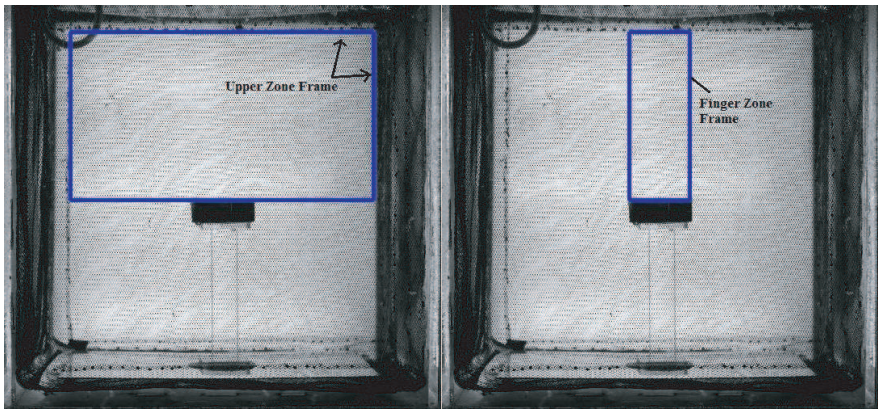

(a) (b)

Figure 5: (a) Study zone, referred to as upper zone, in Intensity Summation Analysis and (b) study zone, referred to as finger zone, in the "finger-height analysis".

3.6.2. Fingers' Characteristics

Several other characteristic parameters were calculated to understand the shape of each finger. These characteristic parameters include finger height and width. A finger zone is defined in images (e.g., Figure 3(b)), which includes the main dye finger for the majority of the time during the upward flow of the dye, when the medium is electromagnetically stimulated at 65 MHz (at 10, 20, and 30 W power levels). This study is limited to the tests performed at 65 MHz because of stronger, more controlled finger movements at this specific frequency. The number of pixels containing enough dye (above a consistent threshold representing visible fingers) was recorded versus elevation within the selected zone at different times. The number represents the width of the finger. This method enabled a study of the finger-width profile for each test over time.As seen in Figure 6(c), the finger for the test performed at 65 MHz at 10 W of power was almost constant at all elevations and was always smaller than the number for 20 and 30 W power levels. For the 20-W case, the finger width was almost constant at all elevations as well but was larger than that of the 10-W case. This was a representative of a more concentrated upward dye flow compared to the 10-W case that was not focused and dispersed gradually. For the test at 30 W, the plot shows that the width decreased rapidly with increasing elevation above the injection cup. However, the fingers became darker (the intensity of these pixels increased drastically). The digital pictures associated with this test confirms much darker, yet more focused, fingers tend to move faster and in a more straight, focused,

and robust shape at 30 W.

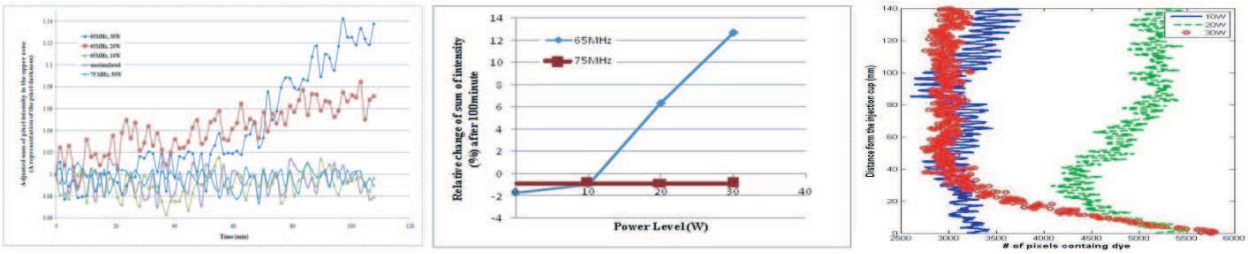

(a) (b) (c)

Figure 6: Plot of adjusted sum of image pixel intensities (representing transported dye amounts) for an unstimulated test; three stimulated tests at 65 MHz at power levels of 10 W, 20 W, and 30 W; and a stimulated test at 75 MHz and 30 W of power versus: (a) time and (b) power (summation performed over highlighted upper zone in digital images); and (c) Plot of total number of pixels containing enough dye to be considered a finger accumulated over time versus elevation above injection cup.

ACKNOWLEDGMENT

This project was supported by the National Science Foundation through the Interdisciplinary Research (IDR) program, CBET Award No. 0928703.

REFERENCES

1. Johnson, R. L., P. C. Johnson, D. B. McWhorter, R. E. Hinchee, and I. Goodman, "An overview of in-situ air sparging," *J. of Groundwater Monitoring and Remediation*, Vol. 13, No. 4, 127–135, 1998.
2. Braida, W. and S. K. Ong, "Air sparging Effectiveness: Laboratory characterization of air-channel mass transfer zone for VOC volatilization," *J. of Hazardous Materials*, Vol. B87, 241–258, 2001.
3. Jones, T. B., "Basic theory of dielectrophoresis and electrorotation," *IEEE Eng. Med. Biol. Mag.*, Vol. 22, No. 6, 33–42, Nov.–Dec. 2003.
4. Azad, M., H. Sangrey, A. Farid, J. Browning, and E. Barney-Smith, "Electromagnetic stimulation of two-phase transport in water-saturated media for geoenvironmental applications," *ASTM, Geotechnical Testing Journal,* Vol. 13, No. 1, 97–106, January 2013.